CHARACTERISTICS AND SPECTRAL EFFECTS OF IRON NANOPARTICLES DURING SPACE WEATHERING OF IRON-RICH OLIVINE. Jing-Yan Xu[1,2], Bing Mo[2,3,4,5], Yan-Xue Wu[6], Hong-Lei Lin[7], Yang Li[2,5], Chao Qi[7,4], Yu-Yan Sara Zhao[2,5]*, Shi-Ling Yang[8], Shen Liu[1]*, Xiong-Yao Li[2,5], Jian-Zhong Liu[2,5]. [1]Northwest University, Xi'an, China; [2]Center for Lunar and Planetary Sciences, Institute of Geochemistry, CAS, Guiyang, China; [3]State Key Laboratory of Ore Deposit Geochemistry, Institute of Geochemistry, CAS, Guiyang, China; [4]College of Earth and Planetary Sciences, University of Chinese Academy of Sciences, Beijing, China; [5]CAS Center for Excellence in Comparative Planetology, Hefei, 230026, China; [6]Analysis and Test Center, Guangdong University of Technology, Guangzhou, China; [7]Key Laboratory of Earth and Planetary Physics, Institute of Geology and Geophysics, CAS, Beijing, China; [8]Key Laboratory of Cenozoic Geology and Environment, Institute of Geology and Geophysics, CAS, Beijing, China. (*Emails: zhaoyuyan@mail.gyig.ac.cn; liushen@nwu.edu.cn)

Introduction: Nanophase metallic Fe (np-Fe^0) particles are ubiquitously present in surface materials on airless celestial bodies subjected to long-term space weathering [1-3]. Previous studies have suggested that np-Fe^0, with various sizes and quantities, can substantially influence the reflectance spectra of airless bodies. Inconsistent observations of the size of np-Fe0 particles and spectral changes have been reported. For instance, some studies suggest that small (<40 nm) np-Fe^0 particles may cause systematic redness and darkening of the spectra, and larger (>40 nm) np-Fe^0 particles may result in darkening of the entire wavelength range but not reddening [4-6]. Analysis of lunar soils and experimental simulants show that nanoparticles <5 nm would cause the spectral reflectance redden, whereas particles >10 nm would result in darkening of the overall reflectance [7].

Of all the rock-forming minerals of basaltic celestial bodies, olivine has the most significant response to space weathering, producing substantial np-Fe^0 particles and resulting in spectral changes [8]. Previous studies using laser irradiation to simulate micrometeorite impacts on the olivine surface focused mainly on Mg-rich olivine (forsterite). However, with Fe-rich olivine detected in the returned lunar regolith by Chang'E-5 [9,10] and the possible presence of Fe-rich olivine on the surface Phobos if it originated from a giant impact of Mars [4], it is of interest to explore how the initial Fe contents in olivine would affect the size and quantities of the formed np-Fe^0 particles. In addition, how these microscopic characteristics of np-Fe^0 particles would affect spectral characteristics, such as Raman and infrared spectroscopy.

Using a set of synthetic Fe-rich olivine samples (Fa100, Fa71, Fa50, Fa30), we conduct laser irradiation experiments to simulate the micrometeorite impacts on Phobos and the Moon. Synthetic Fe-rich olivine samples have fewer impurities than natural olivine and are thus suitable for use as standards to investigate the potential correlation in Fe contents, impact energy, np-Fe^0 particle characteristics, and the corresponding spectroscopic signatures. This simulation work provides new insights into the space weathering of Fe-rich olivine at different locations across the solar system. It may also aid future exploration of Phobos and analysis of lunar regolith samples returned by Chang'E-5.

Synthetic olivine and experimental methods: Four Fe-rich olivine samples (Fa100, Fa71, Fa50, Fa30; Table 1) were synthesized [11]. Olivine powders (< 75 μm) were dried at 80 °C for 8 h and compressed to tablets (13 mm diameter and 2 mm thickness) for use as laser irradiation targets.

Laser irradiation was used to simulate the micrometeorite impacts on the olivine surface. The laser wavelength was 532 nm, the pulse time was 6 ns, and the laser beam spot diameter was focused to 0.5 mm. The experimental chamber has a vacuum degree of $1.8*10^{-4} \sim 2.4*10^{-4}$ Pa. The impact energy conditions were set based on the impact speed of micrometeorites at the Phobos and the Moon (Table 2) [12-15]. The calculated impact energy is 2.23~178 mJ at Phobos and 69.6~139 mJ at the Moon.

Taking into account the energy loss of the lens and cover glass in our simulation system, we set the single-shot energy to 5 mJ for Phobos and 15 mJ for the Moon. Different shot times at one spot were used to simulate different exposure lengths (Table 2).

After laser irradiation, the altered surfaces of the olivine samples were analyzed using Raman and infrared spectroscopy. Then, FIB ultrathin sections were taken from the altered surface and characterized with transmission electron microscopy (TEM) for np-Fe^0 particles and the altered layers.

Table 1. Initial compositions of synthetic olivine.

Fa#	FeO wt%	MgO wt%	SiO_2 wt%	Al_2O_3 wt%	CaO wt%	MnO wt%	Ni wt%
Fa100	70.9	0.01	27.8	0.06	0.25	0.03	0.03
Fa71	54.8	12.5	31.0	0.07	0.22	0.05	0.06
Fa50	41.6	23.3	33.2	0.19	0.24	0.16	0.08
Fa30	26.3	35.8	35.9	0.26	0.32	0.11	0.23

*Note. Fa# is calculated using Fe/(Fe+Mg)*100.*

Table 2. Parameter settings of laser irradiations.

Targets	Single-shot energy	Shot times	Total energy
Phobos Impact speed 8.62 ~ 12 km/s	5 mJ	1	5 mJ
		5	25 mJ
		15	75 mJ
The Moon Impact speed 15 km/s	15 mJ	5	75 mJ
		10	150 mJ

Preliminary results: Fe-rich Fa100 and Mg-rich Fa30 after irradiation at 5 mJ are shown in Fig. 1. The TEM images show that on the rim of Fa100 olivine, there is an amorphous layer (260 nm in thickness) on top of the crystalline boundary (Fig. 1b). No vapor-deposition layer is identified, but depositional bumps are present as ejecta, composed of polycrystalline Fe-oxide (100~300 nm) on top of the amorphous layer (Fig. 1b; Fig. 2). In Fa30, both a vapor deposition layer (30 nm in thickness) and an amorphous layer (110 nm in thickness) are present (Fig. 1e). The altered rim of Fa30 is thinner than that of Fa100.

The np-Fe^0 particles produced by Fa100 and Fa30 are distinctive in size, quantity and distribution. Fa100 produces np-Fe^0 particles that are large in size (~20 nm) but only sporadically distributed along the bottom of the amorphous layer (Fig. 1b). In contrast, Fa30 produces abundant np-Fe^0 particles that are small in size (< 5 nm) and distributed as belts in both the amorphous layer and the vapor-deposition layer (Fig. 1e). At the bottom of the amorphous layer, np-Fe^0 particles formed by direct emergence from the crystalline olivine boundary, consistent with the in situ reduction of olivine due to thermal alteration [16]. The np-Fe^0 particles were distributed in the upper parts of the vapor-deposition layer, consistent with the vaporization-deposition formation mechanism [17,18].

In addition, Ni is present in our initial olivine samples (Table 1), so Ni enrichment in the newly formed np-Fe^0 is expected. At present, we are still looking for signs of Ni enrichment in the products (TEM-EDS detection limit of Ni ~0.1 wt%).

Data analyses of laser-irradiated olivine bearing different initial Fe and different irradiation energies are ongoing. We will report the completed results at the conference.

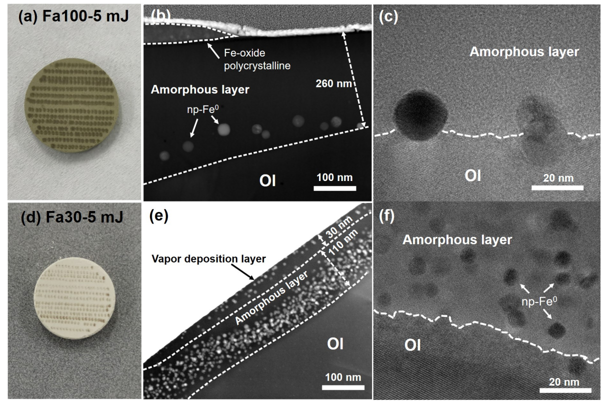

Fig. 1. (a-c) Fa100-5mJ experiment. (a) Target tablet of Fa100 with dark-toned irradiation spots. (b) TEM image of the amorphous layer and np-Fe^0 in Fa100. (c) Enlarged image of (b) showing that np-Fe^0 particles directly emerge from olivine. (d-f) Fa30-5mJ experiment. (d) Target tablet of Fa30 with dark-toned irradiation spots. (e) TEM image of altered layers and np-Fe^0 particles in Fa30. (f)Enlarged image of (e).

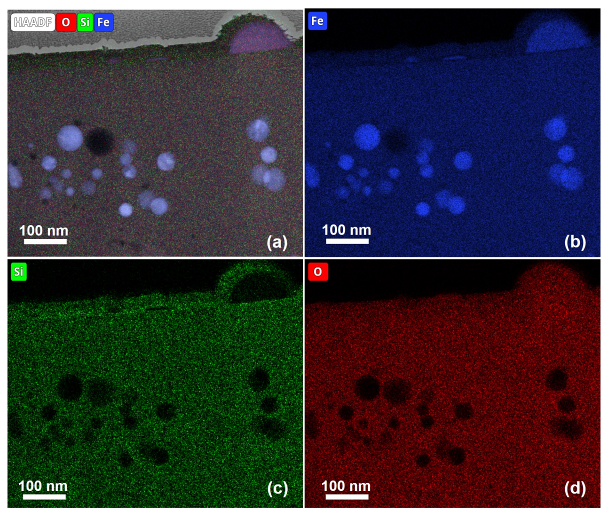

Fig. 2. TEM-EDS mapping shows np-Fe0 particles and polycrystalline Fe-oxide bumps in the Fa100-5mJ experiment. (a)HAADF; (b) Fe; (c) Si; (d)O.

References: [1] Wang, K. et al. (2012) *Earth Planet. Sci. Lett,* 337–338, 17–24. [2] Tucker, W. C. et al. (2018) *Icarus,* 299, 502-512. [3] Gaffey, M.J. (2010) *Icarus,* 209 (2), 564–574. [4] Pieters, C. M. et al. (2016) *JGR*, 121(10), 1865-1884. [5] Noble, S. K. et al. (2007) *Icarus,* 192(2), 629-642. [6] Burgess, K. D. et al. (2018) *JGR,* 123(8), 2022-2037. [7] Thompson, M. S. et al. (2016) *Meteorit. Planet. Sci.,* 51(6), 1082-1095. [8] Sasaki, S. et al. (2001) *Nature,* 410(6828), 555-557. [9] Tian, H. C. et al. (2021) *Nature,* 600(7887), 59-63. [10] Li, Q. L. et al. (2021) *Nature,* 600(7887), 54-58. [11] Qi, C. et al. (2021) *JGR-Soild Earth,* 126,3. [12] Altobelli, N. et al. (2019) *JGR*, 124(4), 1044-1083. [13] Divine, N. (1993) *JGR*, 98(E9), 17029-17048. [14] Ivanov, B. A. (2001) *Space Sci. Rev.,* 96(1), 87-104. [15] Ivanov, B. (2008) *Catastrophic events caused by cosmic objects,* 91-116. [16] Thompson, M. S. et al. (2017) *Meteorit. Planet. Sci., 52*(3), 413-427. [17] Anand, M. et al. (2004) *PNAS*, *101*(18), 6847-6851. [18] Hapke, B. et al. (1975) *The moon*, *13*(1-3), 339-353.